Slow Dynamics in Folded and Unfolded States of an SH3 Domain

Martin Tollinger,[†] Nikolai R. Skrynnikov,[‡] Frans A. A. Mulder,[‡] Julie D. Forman-Kay,[†,§] and Lewis E. Kay*[,‡,§]

Contributions from the Structural Biology and Biochemistry Program, Hospital for Sick Children, Toronto, Ontario, Canada M5G 1X8, Protein Engineering Network Center of Excellence and Departments of Medical Genetics and Chemistry, University of Toronto, Toronto, Ontario, Canada M5S 1A8, and Department of Biochemistry, University of Toronto, Toronto, Ontario, Canada M5S 1A8

Received May 29, 2001. Revised Manuscript Received August 8, 2001

Abstract: ^{15}N relaxation dispersion experiments were applied to the isolated N-terminal SH3 domain of the *Drosophila* protein drk (drkN SH3) to study microsecond to second time scale exchange processes. The drkN SH3 domain exists in equilibrium between folded (F_{exch}) and unfolded (U_{exch}) states under nondenaturing conditions in a ratio of 2:1 at 20 °C, with an average exchange rate constant, k_{ex}, of 2.2 s^{-1} (slow exchange on the NMR chemical shift time scale). Consequently a discrete set of resonances is observed for each state in NMR spectra. Within the U_{exch} ensemble there is a contiguous stretch of residues undergoing conformational exchange on a μs/ms time scale, likely due to local, non-native hydrophobic collapse. For these residues both the $F_{exch} \leftrightarrow U_{exch}$ conformational exchange process and the μs/ms exchange event within the U_{exch} state contribute to the ^{15}N line width and can be analyzed using CPMG-based ^{15}N relaxation dispersion measurements. The contribution of both processes to the apparent relaxation rate can be deconvoluted numerically by combining the experimental ^{15}N relaxation dispersion data with results from an ^{15}N longitudinal relaxation experiment that accurately quantifies exchange rates in slow exchanging systems (Farrow, N. A.; Zhang, O.; Forman-Kay, J. D.; Kay, L. E. *J. Biomol. NMR* **1994**, *4*, 727−734). A simple, generally applicable analytical expression for the dependence of the effective transverse relaxation rate constant on the pulse spacing in CPMG experiments has been derived for a two-state exchange process in the slow exchange limit, which can be used to fit the experimental data on the global folding/unfolding transition. The results illustrate that relaxation dispersion experiments provide an extremely sensitive tool to probe conformational exchange processes in unfolded states and to obtain information on the free energy landscape of such systems.

Introduction

The structural and dynamic characterization of the ensemble of conformations in unfolded states of proteins can provide valuable information on the nature of the free energy landscape of these molecules. The molecular motions of unfolded and partially unfolded proteins are highly heterogeneous, with dynamic processes occurring on multiple time scales.[1] Solution NMR spin relaxation measurements provide a powerful tool for investigating dynamic properties of proteins over a wide range of time scales.[2−4] The majority of NMR spectroscopic studies characterizing the dynamic processes in unfolded states of proteins have focused on very fast time scale motions (ps to ns),[5−13] while relatively few studies have reported on slower (μs to s) time scale dynamics.[14] It is clear, however, that μs to ms conformational exchange processes are an inherent feature of disordered states of proteins, since significant line broadening is often observed in NMR spectroscopic studies of these molecules, reflective of slow interconversion between structures populating local minima on the energy surface.[15−19] Conformational exchange on a μs to ms time scale leads to a modulation of the chemical shift of the affected nuclei, resulting in an increased contribution, R_{ex}, to the effective transverse relaxation rate constant, R_2, and concurrent line-broadening.[20] By measuring R_{ex} as a function of variable pulse spacing in CPMG

[†] Structural Biology and Biochemistry Program, Hospital for Sick Children.

[‡] Protein Engineering Network Center of Excellence and Departments of Medical Genetics and Chemistry, University of Toronto.

[§] Department of Biochemistry, University of Toronto.

(1) Dyson, H. J.; Wright, P. E. *Nat. Struct. Biol.* **1998**, *5*, 499−503.
(2) Palmer, A. G. *Curr. Opin. Struct. Biol.* **1997**, *7*, 732−737.
(3) Kay, L. E. *Nat. Struct. Biol.* **1998**, *5*, 513−517.
(4) Ishima, R.; Torchia, D. A. *Nat. Struct. Biol.* **2000**, *7*, 740−3.
(5) Farrow, N. A.; Zhang, O.; Forman-Kay, J. D.; Kay, L. E. *Biochemistry* **1995**, *34*, 868−878.
(6) Ochsenbein, F.; Guerois, R.; Neumann, J. M.; Sanson, A.; Guittet, E.; van Heijenoort, C. *J. Biomol. NMR* **2001**, *19*, 3−18.
(7) Buck, M.; Schwalbe, H.; Dobson, C. M. *J. Mol. Biol.* **1996**, *257*, 669−683.
(8) Orekhov, V. Y.; Pervushin, K. V.; Arseniev, A. S. *Eur. J. Biochem.* **1994**, *219*, 887−896.
(9) Lefevre, J. F.; Dayie, K. T.; Peng, J. W.; Wagner, G. *Biochemistry* **1996**, *35*, 2674−2686.
(10) Bhattacharya, S.; Falzone, C. J.; Lecomte, J. T. *Biochemistry* **1999**, *38*, 2577−2589.
(11) Brutscher, B.; Bruschweiler, R.; Ernst, R. R. *Biochemistry* **1997**, *36*, 13043−13053.
(12) Schwalbe, H.; Fiebig, K. M.; Buck, M.; Jones, J. A.; Grimshaw, S. B.; Spencer, A.; Glaser, S. J.; Smith, L. J.; Dobson, C. M. *Biochemistry* **1997**, *36*, 8977−8991.
(13) Eliezer, D.; Yao, J.; Dyson, H. J.; Wright, P. E. *Nat. Struct. Biol.* **1998**, *5*, 148−155.
(14) Barbar, E.; Hare, M.; Daragan, V.; Barany, G.; Woodward, C. *Biochemistry* **1998**, *37*, 7822−7833.
(15) Alexandrescu, A. T.; Abeygunawardana, C.; Shortle, D. *Biochemistry* **1994**, *33*, 1063−1072.
(16) Eliezer, D.; Wright, P. E. *J. Mol. Biol.* **1996**, *263*, 531−538.
(17) Wang, Y.; Shortle, D. *Biochemistry* **1995**, *34*, 15895−15905.
(18) Fong, S.; Bycroft, M.; Clarke, J.; Freund, S. M. *J. Mol. Biol.* **1998**, *278*, 417−429.
(19) Schulman, B. A.; Kim, P. S.; Dobson, C. M.; Redfield, C. *Nat. Struct. Biol.* **1997**, *4*, 630−634.
(20) Palmer, A. G.; Williams, J.; McDermott, A. *J. Phys. Chem.* **1996**, *100*, 13293−13310.

10.1021/ja011300z CCC: $20.00
Published on Web 10/26/2001

experiments,[8,21−23] or as a function of effective spin-lock field strengths,[24−26] relaxation dispersion curves are obtained which then can be further analyzed under the assumption of a simple two-state exchange process. Depending on the time scale of the exchange process, both kinetic (exchange rate constant, k_{ex}) and thermodynamic (populations of the involved states) parameters, along with the chemical shift difference, $\delta\omega$, between the two states, may be extracted. The relative values of k_{ex} and $\delta\omega$ define whether an exchange process is referred to as fast ($k_{ex} \gg \delta\omega$), intermediate ($k_{ex} \approx \delta\omega$), or slow ($k_{ex} \ll \delta\omega$) on the NMR chemical shift time scale.

The isolated N-terminal SH3 domain of the *Drosophila* protein drk (drkN SH3 domain) provides an excellent model for the study of disordered states. Under nondenaturing conditions in aqueous buffer near neutral pH this protein exists in equilibrium between folded (F_{exch}) and unfolded states (U_{exch}) in a 2:1 ratio at 20 °C.[27,28] The interconversion between folded and unfolded states of the drkN SH3 domain is slow on the NMR chemical shift time scale, giving rise to distinct sets of resonances for both the F_{exch} and the U_{exch} states. The rate constants underlying the folding/unfolding transition can be investigated by monitoring the exchange of longitudinal nitrogen magnetization, N_z, as shown previously.[5,29] Recent calculations of the structures contributing to the U_{exch} state ensemble based on the structural data available to date have established that relatively compact structures with nativelike properties are significantly populated in the U_{exch} state.[30,31] In addition to slow exchange with the F_{exch} state, structures belonging to the U_{exch} ensemble also interconvert rapidly (in the fast exchange regime on the chemical shift time scale). Heteronuclear NMR relaxation studies have been used to investigate backbone dynamics in the U_{exch} state by evaluating the spectral density function at a number of frequencies.[5] These studies indicate that the U_{exch} state exhibits extensive and very diverse dynamic behavior relative to the F_{exch} state, with motional properties similar to those of disordered regions in folded proteins.

The aim of the present work is to characterize intermediate to fast time scale conformational exchange processes within the drkN SH3 domain unfolded state ensemble (U_{exch} state). Our motivation to study intermediate time scale dynamics within this unfolded state is based on the significant line-broadening observed for the backbone amide resonances of a contiguous segment of the polypeptide chain in the U_{exch} state (residues 23−28), indicating the presence of local μs to ms time scale dynamics for these residues,[32] in addition to the global folding−unfolding process. In the current study, CPMG-based ^{15}N relaxation dispersion measurements are performed to further analyze and characterize the exchange processes which lead to the line broadening of these resonances in the U_{exch} state of the protein.

The ^{15}N relaxation dispersion measurements performed on the exchanging F_{exch}/U_{exch} sample have allowed the characterization of the slow interconversion process ($\tau_{ex} \approx 500$ ms) between F_{exch} and U_{exch} states denoted by $F \underset{k_{uf}}{\overset{k_{fu}}{\rightleftharpoons}} U$. The general features of relaxation dispersion profiles for slowly exchanging systems are discussed in the context of a simple analytical expression that has been derived describing the dependence of the effective transverse relaxation rate, R_2^{eff}, on the CPMG pulse spacing in the case of a two-state slow exchange process. For residues Leu25−Leu28 an additional intermediate time scale conformational exchange process within the unfolded state ensemble ($\tau_{ex} \approx 500$ μs) has been identified. In this case the dynamic equilibrium can be modeled most simply as $F \underset{k_{uf}}{\overset{k_{fu}}{\rightleftharpoons}} U \underset{k_{u^*u}}{\overset{k_{uu^*}}{\rightleftharpoons}} U^*$ (see below). The results indicate the existence of a locally stable conformational substate (U^*) within the unfolded state ensemble, likely due to non-native hydrophobic collapse.

Results

^{15}N relaxation dispersion measurements were performed on the exchanging (F_{exch}/U_{exch}) sample using a relaxation-compensated CPMG pulse sequence[22] with the CPMG period implemented in a constant time (CT) manner.[23] Effective transverse relaxation rate constants, R_2^{eff}, were measured as a function of the B_1 rf field strength, ν_{CP}, where $\nu_{CP} = 1/(4\tau_{CP})$ with $2\tau_{CP}$ the time between the centers of successive 180° pulses in the CPMG sequence. Figure 1 illustrates the pulse scheme that was used to measure dispersion profiles; the sequence is similar to a recently published experiment for measuring exchange contributions to ^{15}N line widths in AX_2 spin systems,[23] with a small number of modifications required for application to backbone $^{15}N-^{1}H$ spin pairs. Residues in both F_{exch} and U_{exch} states exhibit small but statistically significant exchange contributions, R_{ex}, to the effective transverse relaxation rate, which derive from the global folding/unfolding transition between F_{exch} and U_{exch} states. Figure 2 shows, as representative examples, experimental relaxation dispersion data for resonances Glu16 and Thr22 in the F_{exch} state and for residues Ser10 and Tyr52 in the U_{exch} state. Similar relaxation dispersion curves were found for all residues in the folded state and for all but three residues (see below) in the unfolded state.

Relaxation Dispersion Profiles in the Slow Exchange Limit Can Be Described by a Simple Equation. To extract information on the drkN SH3 domain folding/unfolding transition from the profiles illustrated in Figure 2 an analytical expression has been derived describing the dependence of the effective transverse relaxation rate on τ_{CP} in the slow exchange limit. A two-site exchange process is considered according to the scheme

$$A \underset{k_b}{\overset{k_a}{\rightleftharpoons}} B$$

where the chemical shift difference between sites is $\delta\omega$ (in units of angular frequency), the equilibrium populations of states A and B are p_a and p_b with $p_a + p_b = 1$, and the forward and reverse first-order rate constants are denoted by k_a and k_b, respectively. The exchange rate constant, k_{ex}, is defined as $k_{ex} = k_a + k_b$, and the exchange lifetime as $\tau_{ex} = 1/k_{ex}$.

In work by Allerhand and Gutowsky, an approximate functional form for the dependence of the effective decay rate, R_2^{eff}, on the spacing between 180° pulses in CPMG experi-

(21) Millet, O.; Loria, J. P.; Kroenke, C. D.; Pons, M.; Palmer, A. G. *J. Am. Chem. Soc.* **2000**, *122*, 2867−2877.
(22) Loria, J. P.; Rance, M.; Palmer, A. G. *J. Am. Chem. Soc.* **1999**, *121*, 2331−2332.
(23) Mulder, F. A. A.; Skrynnikov, N. R.; Hon, B.; Dahlquist, F. W.; Kay, L. E. *J. Am. Chem. Soc.* **2001**, *123*, 967−975.
(24) Akke, M.; Palmer, A. G. *J. Am. Chem. Soc.* **1996**, *118*, 911−912.
(25) Mulder, F. A. A.; van Tilborg, P. J.; Kaptein, R.; Boelens, R. *J. Biomol. NMR* **1999**, *13*, 275−288.
(26) Zinn-Justin, S.; Berthault, P.; Guenneugues, M.; Desvaux, H. *J. Biomol. NMR* **1997**, *10*, 363−372.
(27) Zhang, O.; Kay, L. E.; Olivier, J. P.; Forman-Kay, J. D. *J. Biomol. NMR* **1994**, *4*, 845−858.
(28) Zhang, O.; Forman-Kay, J. D. *Biochemistry* **1995**, *34*, 6784−6794.
(29) Farrow, N. A.; Zhang, O.; Forman-Kay, J. D.; Kay, L. E. *J. Biomol. NMR* **1994**, *4*, 727−734.
(30) Mok, Y. K.; Kay, C. M.; Kay, L. E.; Forman-Kay, J. D. *J. Mol. Biol.* **1999**, *289*, 619−638.
(31) Choy, Y.-W.; Forman-Kay, J. D. *J. Mol. Biol.* **2001**, *308*, 1011−1032.
(32) Zhang, O.; Forman-Kay, J. D. *Biochemistry* **1997**, *36*, 3959−3970.

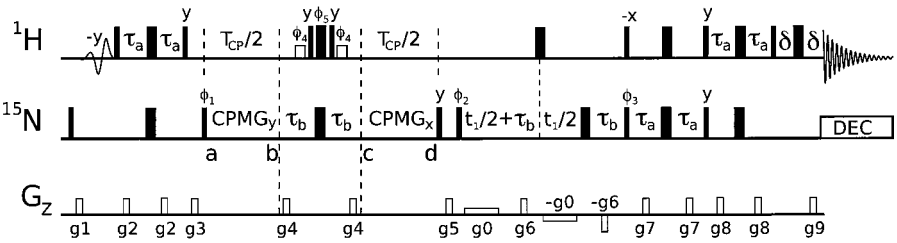

Figure 1. Pulse scheme of the constant relaxation time CPMG dispersion experiment. Narrow (wide) bars correspond to 90° (180°) rf pulses applied with phase *x*, unless indicated otherwise. Filled rectangular ^{1}H pulses are applied with a field of 34 kHz, centered on the water resonance. The shaped ^{1}H pulse at the start of the sequence is a 6.5 ms EBURP-1 pulse to selectively excite the water resonance.[44] The open square bars represent 1.6 ms ^{1}H 90° pulses, applied selectively to the water resonance, as in WATERGATE[45] to ensure that the water magnetization is along the $+z$ axis during both relaxation periods (from a to b and c to d). All ^{15}N pulses between points a and d (including the flanking 90° pulses of phase $\phi 1$ and *y*) are applied with a field strength of 5.5 kHz. CPMG$_\phi$ indicates a string of $n/2$ elements $[\tau_{CP}-180_\phi{}^\circ-\tau_{CP}]$, where $T_{CP}/2 = n/2(2\tau_{CP} + pw_N^{180^\circ})$ and $pw_N^{180^\circ}$ is the nitrogen 180° pulse width. All other ^{15}N pulses are applied with a field of 6.3 kHz. A 1 kHz (500 and 600 MHz) or 1.5 kHz (800 MHz) Waltz16 decoupling field[46] is applied during acquisition. Values of the delays are: $\tau_a = 2.25$ ms; $\tau_b = 1/(4J_{NH}) = 2.677$ ms; $\delta = 0.5$ ms; $T_{CP} = 80.0$ ms. The phase cycling employed is $\phi_1 = \{x, -x\}$, $\phi_2 = 4\{y\},4\{-y\}$, $\phi_3 = \{x\}$, $\phi_4 = 2\{x\},2\{-x\}$, $\phi_5 = 2\{-x\},2\{x\}$, $\phi_{rec} = 2\{x, -x\},2\{-x, x\}$. Gradient strengths in G/cm (lengths in ms) are $g0 = 0.5$ ($t_1/2$), $g1 = 5.0$ (1.0), $g2 = 4.0$ (0.5), $g3 = -6.0$ (1.0), $g4 = 18.0$ (0.5), $g5 = 15.0$ (0.8), $g6 = 15.0$ (1.1), $g7 = 3.5$ (0.4), $g8 = 2.5$ (0.3), $g9 = 28.9$ (0.11). For each t_1 increment axial peaks are shifted to the border of the spectrum by inversion of ϕ_2 in concert with the receiver phase.[47] Quadrature detection in F_1 is achieved by the enhanced sensitivity approach whereby separate sets of spectra corresponding to ($\phi 3$, $g9$) and ($\phi 3 + 180^\circ$, $-g9$) are recorded for each value of t_1.[48,49]

ments was derived for systems comprised of two exchanging sites with arbitrary equilibrium populations but equal spin−spin relaxation rates, R_2.[33] These results were later extended by Carver and Richards, who derived a similar expression without the restrictive assumption of equal spin−spin relaxation rates for the two sites.[34] In both cases, the decay in echo amplitude for a CPMG pulse train could be described by the sum of two exponential terms. To obtain a relatively simple analytical expression for R_2^{eff}, only one exponential term was retained, giving the expression (for the more populated site *A* in the above exchange scheme):[34,35]

$$R_{2a}^{eff} = \frac{1}{2}\left(R_{2a} + R_{2b} + k_a + k_b - \frac{1}{2\tau_{CP}}\cosh^{-1}[D_+\cosh(\eta_+) - D_-\cos(\eta_-)]\right) \quad (1)$$

where

$$D_\pm = \frac{1}{2}\left[\pm 1 + \frac{\psi + 2\delta\omega^2}{(\psi^2 + \xi^2)^{1/2}}\right]$$

$$\eta_\pm = \sqrt{2}\tau_{CP}[\pm\psi + (\psi^2 + \xi^2)^{1/2}]^{1/2}$$

$$\psi = (R_{2a} - R_{2b} + k_a - k_b)^2 - \delta\omega^2 + 4k_ak_b$$

$$\xi = 2\delta\omega(R_{2a} - R_{2b} + k_a - k_b)$$

and R_{2a}, R_{2b} are transverse relaxation rates of spins in sites *A* and *B* in the absence of exchange.

Allerhand and Gutowsky[33] and later Carver and Richards[34] showed analytically that the decay can be well approximated by a single exponential in the case of fast or intermediate exchange but not for slow exchange. In the latter case significant discrepancies between exact numerical values of R_2^{eff} and rates calculated from eq 1 above can be found in regions where oscillations in the plots of R_2^{eff} versus the CPMG field strength occur[33] (see below). Here we derive an expression for the dependence of R_2^{eff} on τ_{CP} which is applicable in the limit of slow exchange and when $|R_{2a} - R_{2b}| \ll k_a,k_b \ll 1/\tau_{CP}$ (see Appendix) that correctly represents the oscillations observed in the slow pulsing limit.

As described in the Appendix the derivation is based on a first-order perturbation theory solution of the equations of evolution of the spin density matrix (equivalent to the Bloch equations) which include magnetization transfer effects due to chemical exchange.[36] The analytical expression obtained for the dependence of R_2^{eff} on the CPMG pulse spacing in the slow exchange limit is (for site *A* in the above exchange scheme):

$$R_{2a}^{eff} = R_{2a} + k_a - k_a\frac{\sin(\delta\omega\tau_{CP})}{\delta\omega\tau_{CP}} \quad (2)$$

where R_{2a} is the transverse relaxation rate of site *A* in the absence of exchange (resulting from mechanisms such as dipolar or CSA interactions) and $2\tau_{CP}$ is the time between successive 180° pulses. Plots of the dependence of R_2^{eff} on the CPMG field strength, ν_{CP}, are shown for various values of $\delta\omega$ and k_a in Figure 3, focusing on the exchange contribution to the effective transverse relaxation rate (i.e. assuming $R_{2a} = R_{2b} = 0$).

Since eq 2 is rather simple, it is very useful for illustrating the major functional features of dispersion curves in the slow exchange regime. A particularly interesting feature of the dispersion curves shown in Figure 3 is the damped oscillations, which occur at low CPMG field strengths (slow pulsing limit). The frequency of the oscillations is determined by the sinusoidal term in eq 2 and is solely a function of the chemical shift difference between the two sites (i.e., independent of the rate of exchange). Extrema of the sinc($\delta\omega\tau_{CP}$) term occur for $\tau_{CP} = (1/\delta\omega)\tan(\delta\omega\tau_{CP})$.

Figure 4 illustrates the physical origin of the oscillations predicted by eq 2 and shown in Figure 3. Without loss in generality we have assumed that (i) spin *A* is on resonance, while spin *B* evolves at a frequency offset of $\delta\omega$ with respect to *A*, that (ii) *A* and *B* spin magnetization is initially along the *x*-axis, and that (iii) the intrinsic relaxation rates of magnetization at sites *A* and *B* are equal. Suppose for a moment that refocusing

(33) Allerhand, A.; Gutowsky, H. S. *J. Chem. Phys.* **1965**, *42*, 1587−1599.
(34) Carver, J. P.; Richards, R. E. *J. Magn. Reson.* **1972**, *6*, 89−105.
(35) Davis, D. G.; Perlman, M. E.; London, R. E. *J. Magn. Reson.* **1994**, *B104*, 266−275.
(36) McConnell, H. M. *J. Chem. Phys.* **1958**, *28*, 430−431.

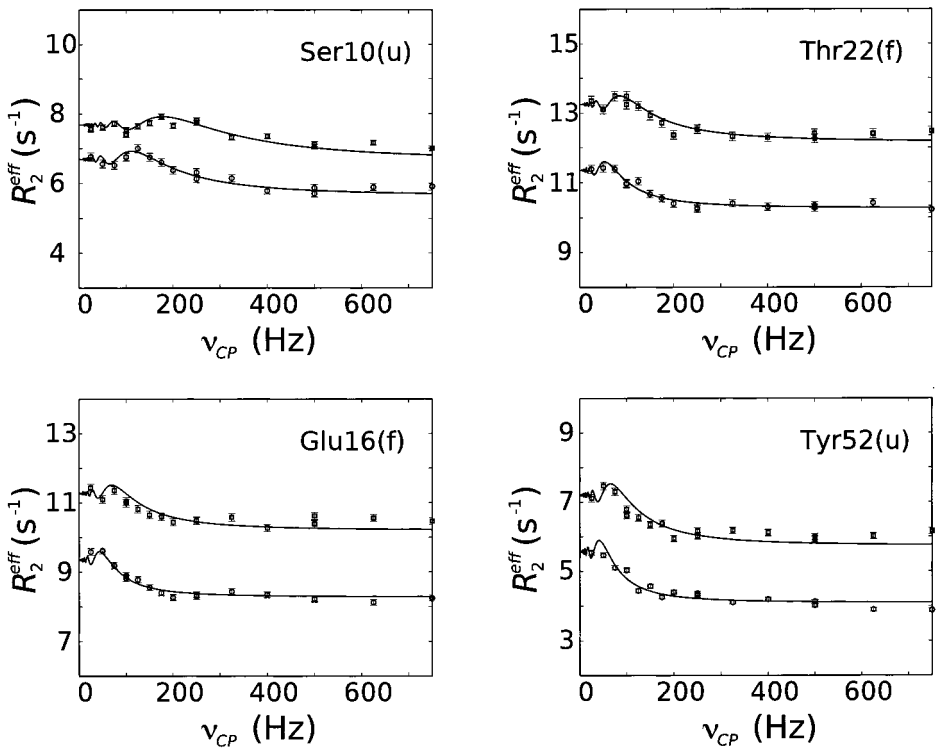

Figure 2. Effective transverse ^{15}N relaxation rates, R_2^{eff}, as a function of the CPMG field strength, ν_{CP}, for Ser10 in the U_{exch} state, Glu16 (F_{exch}), Thr22 (F_{exch}), and Tyr52 (U_{exch}). The best-fit dispersion curves using eq 2 are shown (solid lines). Data recorded at 800 (500) MHz ^{1}H Larmor frequency are indicated with squares (circles). Dispersion profiles have also been measured at 600 MHz (not shown) and used in all analyses. Error bars are estimated from the repeat experiments. Values of $\delta\omega_{rex}$ ($\delta\omega_{UF}$) for these residues are [ppm]: 6.27 (6.20) for Ser10, 2.45 (2.19) for Glu16, 3.00 (3.30) for Thr22, 2.31 (1.76) for Tyr52.

pulses are not applied (free precession limit). Due to the difference in chemical shifts a phase difference between the two vectors, M_a and M_b, describing the magnetization of spins *A* and *B*, respectively, is generated and the instantaneous flow of *x*-magnetization from site *B* to *A* due to exchange can therefore be positive (the pair of vectors is in-phase; that is, the projection of vector *B* on *A* is positive), zero (the two vectors are orthogonal) or negative (the pair of vectors is anti-phase; that is, the projection of vector *B* on *A* is negative). Averaged over an integral number of precession cycles the net transfer of magnetization from *B* to *A* is zero, and the effect of exchange is simply to increase the rate of decay of M_a by k_a (due to the flow of magnetization from *A* to *B*).

The situation when refocusing pulses are applied is more complex as shown in Figure 4 where the evolution of magnetization at sites *A* and *B* during the period $\tau_{\text{CP}}-180°-2\tau_{\text{CP}}-180°-\tau_{\text{CP}}$ is illustrated. In this example we have considered the case where the relative phase between M_a and M_b immediately prior to the application of the first 180° pulse is $\delta\omega\tau_{\text{CP}} = 3\pi/2$ (top part of the figure). The middle panel illustrates the time dependence of the *x*- and *y*-components of M_b during the course of the sequence, while the net amount of magnetization accumulated at site *A* due to transfer from *B* is illustrated in the bottom portion of the diagram. It is noteworthy that the net amount of *x*-magnetization transferred at the end of a $\tau_{\text{CP}}-180°-2\tau_{\text{CP}}-180°-\tau_{\text{CP}}$ interval is negative (bottom part of the plot). Consequently, the amplitude of magnetization $M_{a,x}$ detected at the end of this period is reduced, which results in an increased R_2^{eff} value. The situation illustrated in Figure 4 corresponds to the largest maximum in the R_2^{eff} profile (see Figure 3, a and b), which is the first maximum in the dispersion curve from right to left, occurring at $\delta\omega\tau_{\text{CP}} \approx 3\pi/2$. Note that there is no net transfer of *y*-magnetization from site *B* to *A* in this same period.

If, however, the relative phase difference between M_a and M_b prior to the application of the first 180° pulse is $\delta\omega\tau_{\text{CP}} = (n + 1)\pi$ magnetization will not accumulate at site *A* due to transfer from *B* and $R_{2a}^{\text{eff}} = R_{2a} + k_a$. Further, if $\delta\omega\tau_{\text{CP}} = (2n + 1/2)\pi$ the amplitude of $M_{a,x}$ detected at the end of the $\tau_{\text{CP}}-180°-2\tau_{\text{CP}}-180°-\tau_{\text{CP}}$ period due to transfer from site *B* is increased, leading to a decreased R_2^{eff} value. For other values of $\delta\omega\tau_{\text{CP}}$ there is either an increase or decrease in R_2^{eff} (depending on the value of τ_{CP}), resulting in the observed oscillations in $R_2^{\text{eff}}(\nu_{\text{CP}})$. It is interesting that the amplitude of the oscillations scales linearly with k_a at any CPMG field strength. Hence, the remarkable situation arises that the effective relaxation rate, R_2^{eff}, can be considerably higher at nonzero CPMG field strengths than in the free precession limit at $\nu_{\text{CP}} = 0$.

The existence of the damped oscillations at low CPMG field strengths can indeed be verified experimentally for the slow exchange between unfolded and folded states of the drkN SH3 domain, as shown in Figure 2. The oscillations are particularly pronounced in dispersion profiles of residues where the chemical shift difference between the exchanging sites is large, such as in Ser10, since in this case it is possible to obtain a good sampling of the dispersion curve in the region $\nu_{\text{CP}} \ll \delta\omega$.

As noted previously,[21,37] the chemical exchange contribution to transverse relaxation, R_{ex}, defined as the difference between the apparent transverse relaxation rate in the slow and fast pulsing limits, $R_{\text{ex}} = [R_2^{\text{eff}}(1/\tau_{\text{CP}} \rightarrow 0) - R_2^{\text{eff}}(1/\tau_{\text{CP}} \rightarrow \infty)]$, is independent of $\delta\omega$ and, hence, of the static magnetic field strength, B_0, in the slow exchange limit. Equation 2 clearly shows that R_{ex} is indeed independent of $\delta\omega$ but is solely determined by the forward rate constant ($R_{\text{ex}} = k_a$) in the limit of slow exchange. Another useful parameter is the half-step

(37) Ishima, R.; Torchia, D. A. *J. Biomol. NMR* **1999**, *14*, 369−372.

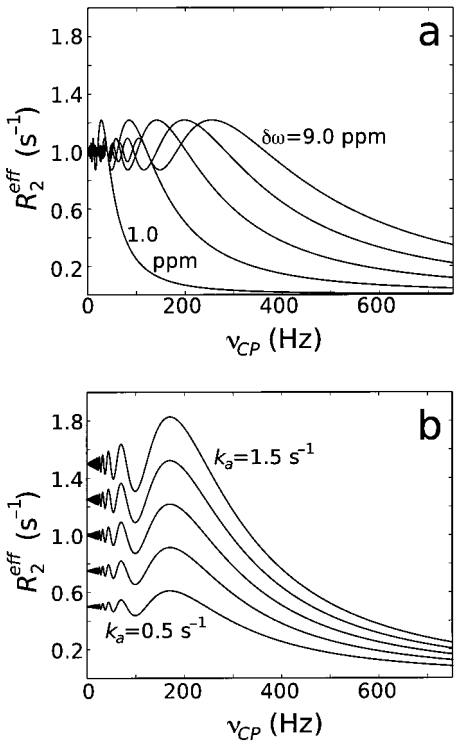

Figure 3. Theoretical dispersion curves derived from eq 2 illustrating the dependence of R_2^{eff} on the CPMG field strength, ν_{CP}. The parameters used to simulate the dispersion curves are similar to those characterizing the slowly exchanging drkN SH3 domain. (a) Effect of the chemical shift difference, $\delta\omega$, on relaxation dispersion curves in the slow exchange regime. Simulations assume a forward rate constant (A → B) of $k_a = 1.0$ s^{-1} and the chemical shift difference, $\delta\omega$, is varied from 1.0 to 9.0 ppm in 2.0 ppm steps. (b) Effect of the forward rate constant, $k_a = p_b/\tau_{ex}$, on the relaxation dispersion profile, $R_{2a}^{\text{eff}}(\nu_{\text{CP}})$, assuming $\delta\omega = 6.0$ ppm. Values of k_a [s^{-1}] are: 0.5, 0.75, 1.0, 1.25, and 1.5. The dispersion curves corresponding to state A are shown. Curves were calculated for a ^{1}H Larmor frequency of 800 MHz, and only the exchange contribution to R_{2a}^{eff} is shown (i.e., $R_{2a} = R_{2b} = 0$).

frequency, $\nu_{1/2}$, which is defined as the ν_{CP} value for which half of the exchange contribution to the ^{15}N line width is quenched, that is, $R_2^{\text{eff}} = R_2 + {}^1/_2(R_{\text{ex}})$. From eq 2 it is clear that the half-step in the dispersion curve will occur when $\text{sinc}(0.25\delta\omega/\nu_{1/2}) = 0.5$, which uniquely defines $\nu_{1/2}$. In the slow exchange limit the value of $\nu_{1/2}$ depends, therefore, linearly on the chemical shift difference, $\delta\omega$, and hence on the static magnetic field strength, B_0.

It is important to note that eq 1, in the limit of slow exchange, is not identical to eq 2. Figure 5 compares relaxation dispersion curves, which are calculated using eqs 1 or 2 ($R_{2a} = R_{2b}$) with profiles obtained by solving the system of coupled differential equations that exactly describe the exchange process (see Appendix). Whereas eq 2 describes the dispersion curves correctly, relaxation rates calculated using eq 1 clearly deviate from numerically calculated values. Figure 5a establishes that R_2^{eff} values calculated using eq 2 are in excellent agreement with the exact, numerically calculated values for a slow two-state process with an exchange lifetime of 500 ms (corresponding to $k_{\text{ex}} = 2$ s^{-1}), assuming a chemical shift difference, $\delta\omega$, of 6.0 ppm and variable equilibrium populations of the states. In contrast, eq 1 fails to describe the oscillations correctly and predicts a dependence of $\nu_{1/2}$ on both $\delta\omega$ and the populations of the exchanging states. As mentioned above, the value of the half-step frequency, $\nu_{1/2}$, is solely a function of $\delta\omega$ in the slow exchange limit. It is interesting to note that for this reason eq 1

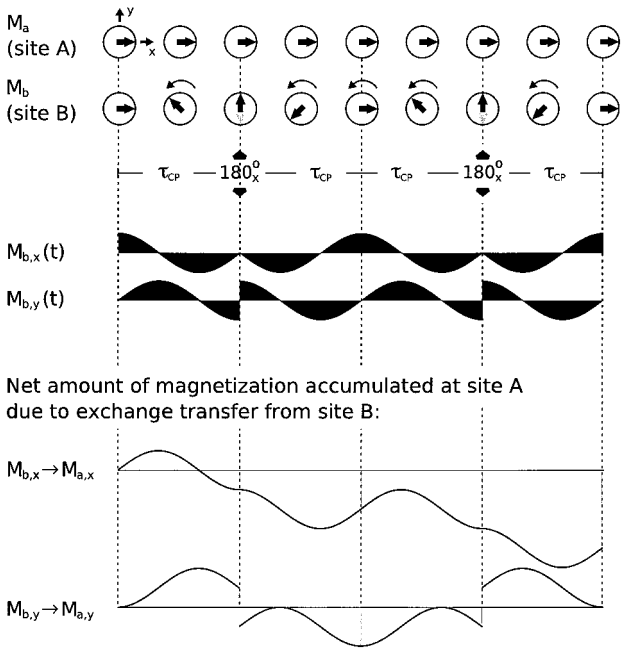

Figure 4. Schematic representation of the evolution of spin magnetization at site *A* through a period, $\tau_{\text{CP}}-180°-2\tau_{\text{CP}}-180°-\tau_{\text{CP}}$, starting from *x*-magnetization, with spin *A* on resonance and spin *B* evolving with a frequency of $\delta\omega$ (top). The middle panel shows the *x*- and *y*-components of magnetization from spin *B* during the course of the sequence, while the bottom panels illustrate the accumulation of magnetization at site *A* due to the transfer, $M_{b,x} \rightarrow M_{a,x}$, $M_{b,y} \rightarrow M_{a,y}$. In this example $\delta\omega\tau_{\text{CP}}$ is chosen to be $3\pi/2$. Note that there is no net accumulation of *y*-magnetization due to exchange (i.e., the net transfer $M_{b,y} \rightarrow M_{a,y}$ is zero).

gives the wrong impression that in the slow exchange case populations, p_a and p_b, and exchange lifetimes, τ_{ex}, can be separated by fitting data from one state measured at multiple static magnetic field strengths. Figure 5b illustrates that eq 2 is still a very good approximation for exchange lifetimes on the order of 100 ms, even in cases of highly skewed site populations (as long as $R_{2a} = R_{2b}$, see Appendix). Simulations establish that when the condition $|R_{2a} - R_{2b}| \ll k_a,k_b$ no longer holds deviations between R_2^{eff} rates predicted by eq 2 and actual values emerge for large ν_{CP} values. For example, for $k_a = k_b = 1$ s^{-1} and $R_{2a} = 10$ s^{-1}, $R_{2b} = 5$ s^{-1} differences of ~0.2 s^{-1} are calculated for $R_{2a}^{\text{eff}}(\nu_{\text{CP}} = 750$ Hz), corresponding to 18% of the total dispersion (1.2 s^{-1}).

Slow Exchange between F_{exch} and U_{exch}. Relaxation dispersion profiles describing the slow exchange between F_{exch} and U_{exch} states have been fit using eq 2 and using an exact analytical formula for $R_2^{\text{eff}}(\nu_{\text{CP}})$ (this formula requires approximately 40 lines, see Appendix) which retains both exponents necessary to describe evolution of magnetization in a two-site, slowly exchanging system. Similar results were obtained with both approaches (essentially identical $\delta\omega$ values and exchange rates that differ by less than 10%, on average), and therefore results from the fit using eq 2 only are reported. As illustrated in Figure 3a, relaxation dispersion curves in the slow two-site exchange limit are very sensitive to the chemical shift difference between the exchanging states, $\delta\omega$. Figure 6 shows the excellent correlation between the ^{15}N chemical shift differences for unfolded and folded states obtained from R_{ex} measurements ($\delta\omega_{rex}$) and directly from the two sets of resonances in spectra of the SH3 domain ($\delta\omega_{UF}$). Slopes of 1.01 and 1.02 are obtained for residues in the U_{exch} and F_{exch} states, respectively. (It is noteworthy that significantly worse correlations were obtained between $\delta\omega_{rex}$

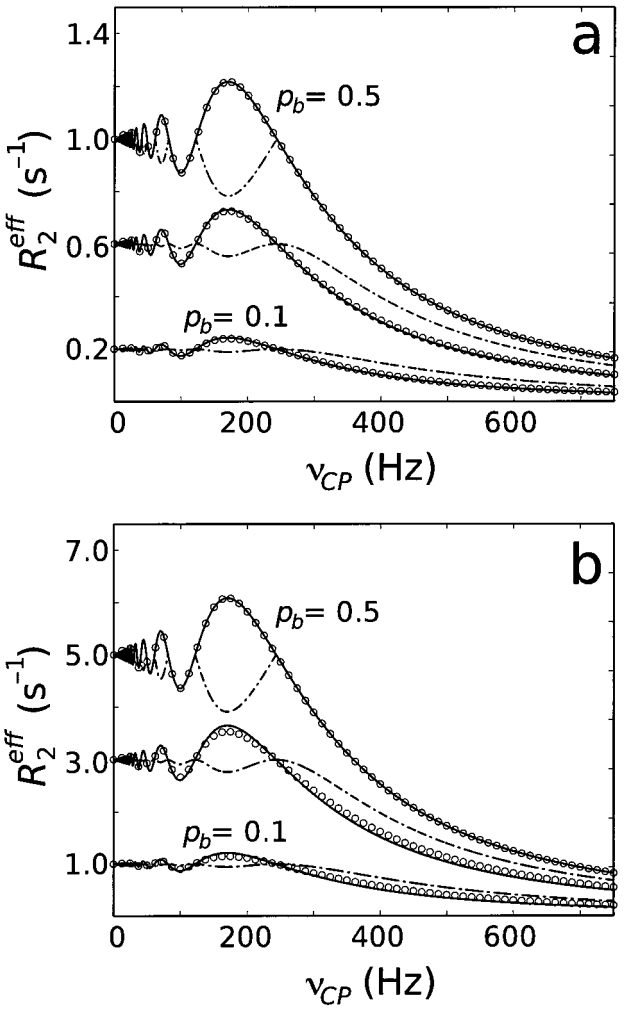

Figure 5. Comparison of relaxation dispersion curves simulated using eq 2 (solid lines) and eq 1 (dash−dotted lines) with values of R_{2a}^{eff} calculated using the exact solution of the Bloch equations including the effects of chemical exchange (circles; see eq A1 and discussion in the Appendix). (a) Values of $p_b = 0.1$, 0.3, and 0.5 and $\tau_{ex} = 500$ ms (corresponding to k_a [s^{-1}] = 0.2, 0.6, and 1.0) have been used. (b) $p_b = 0.1$, 0.3, 0.5, $\tau_{ex} = 100$ ms (corresponding to k_a [s^{-1}] = 1.0, 3.0, 5.0). All plots were prepared assuming $\delta\omega = 6.0$ ppm and a ^{1}H Larmor frequency of 800 MHz. Only the contribution to R_{2a}^{eff} due to exchange is shown (i.e., $R_{2a} = R_{2b} = 0$).

and $\delta\omega_{UF}$ when eq 1 was used to fit the data, with slopes on the order of 0.8.) Residues with $\delta\omega_{UF} < 1.0$ ppm were omitted from the analysis because it is not possible to obtain a sufficient sampling of the relaxation dispersion curve in the region $\nu_{CP} < \nu_{1/2}$. Note that for the ν_{CP} values used in the experiments ($\nu_{CP} \geq 25$ Hz; see Materials and Methods) and $\delta\omega_{UF} = 1.0$ ppm, $\nu_{1/2}$ is 42.0 Hz for data recorded at 500 MHz. Conversely, parameters extracted from dispersion profiles for residues with $\delta\omega_{UF} > 9.0$ ppm are error prone because the CPMG field strengths employed in our experiments ($\nu_{CP} < 750$ Hz) are not sufficiently high to allow measurable changes of R_2^{eff} with ν_{CP} in the high-field region of the relaxation dispersion curve.

Note that for slow exchange the R_{ex} contributions to R_2^{eff} depend only on a single rate constant (on $k_a = p_b k_{ex}$ for the forward reaction) so that the equilibrium populations and the exchange rates cannot be disentangled by analyzing relaxation dispersion curves for only one of the two states. To quantify both populations and exchange rates resonances from the folded and unfolded forms of the SH3 domain must be amenable to analysis.

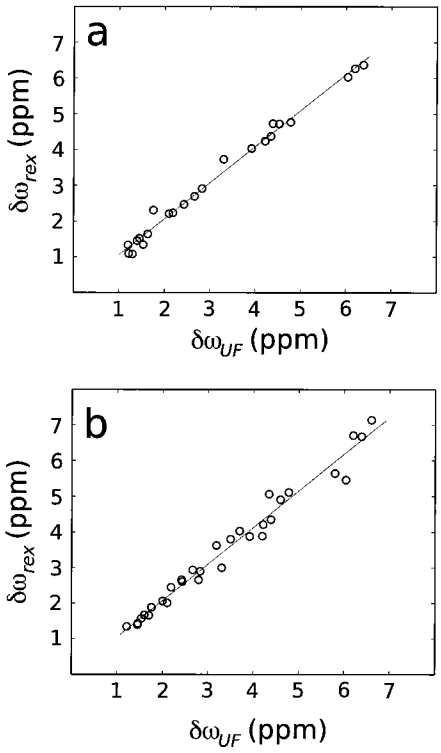

Figure 6. Correlation between $\delta\omega_{rex}$, obtained from fits of dispersion profiles to eq 2, and the actual chemical shift difference, $\delta\omega_{UF}$, obtained directly from HSQC spectra for (a) residues in the U_{exch} state and (b) residues in the F_{exch} state. The pairwise rmsd between $\delta\omega_{rex}$ and $\delta\omega_{UF}$ values are 0.19 and 0.29 ppm for residues in the U_{exch} and F_{exch} states, respectively. Only residues for which 1.0 ppm < $\delta\omega_{UF}$ < 9.0 ppm and with an offset from the ^{15}N carrier of less than 10 ppm (to avoid off-resonance effects) have been used in the analysis. Residues 25−28, which exhibit additional intermediate time scale exchange in the U_{exch} state, are not included in (a).

The slow exchange process between folded and unfolded states in the drkN SH3 domain (exchange rate constant $k_{ex} \approx 2.2$ s^{-1}) can also be investigated by monitoring the exchange of longitudinal nitrogen magnetization, N_z, because in this system the equilibrium populations of both states, F_{exch} and U_{exch}, are large enough to generate observable signals. The details of the experimental approach have been described previously.[29] Briefly, a pair of auto peaks (*ff* and *uu*) is observed for each residue as well as a pair of exchange cross-peaks (*fu* and *uf*), which result from the transfer of magnetization between the folded and unfolded states during the mixing time. This experiment enables the quantitation of slow exchange processes, where separate resonances for the involved states are observed, but not of intermediate-to-fast exchange processes, where only a single resonance line is obtained at the population-weighted average chemical shift. In the exchanging (F_{exch}/U_{exch}) sample, the unfolding and folding rate constants, k_{fu} and k_{uf} (along with the ^{15}N longitudinal relaxation rate constants R_{1f} and R_{1u}) can be determined simultaneously by fitting the experimental data from the N_z experiment to the appropriate analytical expressions which are obtained from solution of the Bloch equations including the effects of chemical exchange[29] (see Materials and Methods). Examples of the experimental data obtained from the N_z experiment together with fitted curves are shown in Figure 7 for the same residues as in Figure 2. Note that in the representation chosen here, that is when the intensities of *ff* (*uu*) auto peaks and *fu* (*uf*) cross-peaks are normalized by the intensity of the *ff* (*uu*) auto peak at zero mixing time, the initial

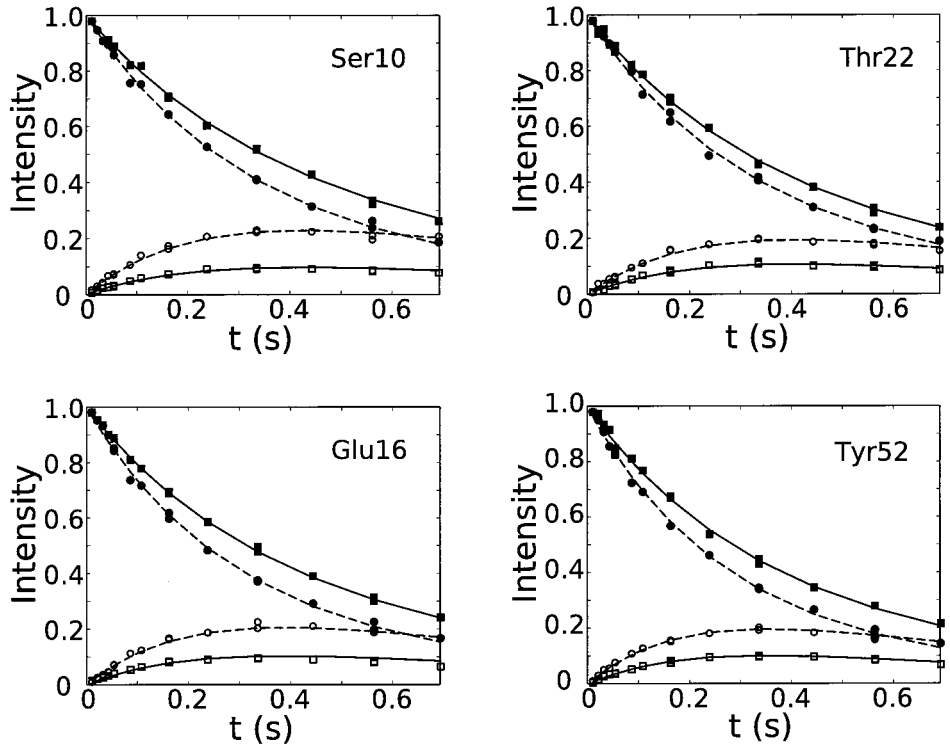

Figure 7. Time profiles of the intensities of the auto (*uu* and *ff*) and exchange (*uf* and *fu*) peaks in the N_z experiment for residues Ser10, Glu16, Thr22, and Tyr52. Solid lines indicate the best-fit curves for magnetization originating in the folded state corresponding to the auto- and cross-peaks, *ff* and *fu*, while dashed lines are the best-fit curves for magnetization originating in the unfolded state (*uu* and *uf*). Solid and open symbols are used to distinguish data derived from the auto peaks and from exchange cross-peaks, respectively. The intensities of *ff* (*uu*) and *fu* (*uf*) correlations are normalized such that the intensity of the *ff* (*uu*) auto peak at zero mixing time is 1.0 and corrected for relaxation during the pulse sequence, as described in Materials and Methods. The folding and unfolding rate constants k_{uf} (k_{fu}) extracted from the data are [s^{-1}]: 1.51 ± 0.24 (0.64 ± 0.06) for Ser10, 1.50 ± 0.25 (0.76 ± 0.02) for Glu16, 1.25 ± 0.10 (0.74 ± 0.09) for Thr22, 1.59 ± 0.13 (0.82 ± 0.07) for Tyr52.

slopes of the buildup curves are equal to the unfolding (folding) rate constants.

Values for the folding and unfolding rate constants, k_{uf} and k_{fu}, which are extracted from the relaxation dispersion data are, in many cases, in qualitative agreement with results from the N_z experiment. Due to the small exchange contributions to the transverse relaxation rates (on average 1.5 s^{-1} for U_{exch} resonances and 0.7 s^{-1} for F_{exch} resonances), however, values extracted from the relaxation dispersion data are much less accurate than those from the N_z experiment. Because the positions of the maxima in the dispersion curves of slowly exchanging spins vary with B_o, accurate $\delta\omega_{rex}$ values can be obtained from fits of dispersion data recorded at a number of different B_o fields. In contrast, exchange rate constants derived from fits of the same data are significantly less accurate.

Intermediate Time Scale Exchange within the U_{exch} Ensemble. Unlike the N_z experiment the CPMG method is sensitive not only to slow but also to intermediate-to-fast time scale exchange processes. As noted by Millet et al., the dependence of the exchange contribution, R_{ex}, on the static magnetic field strength provides a method of distinguishing between slow and fast time scale exchange processes.[21] As discussed above, in the slow exchange limit R_{ex} is independent of the chemical shift difference (and hence of the static magnetic field strength, B_o), whereas generally R_{ex} depends on $\delta\omega$ and scales quadratically with the static magnetic field strength in the limit of fast exchange. A plot of $\Delta R_{ex} = R_{ex}(800\ MHz) - R_{ex}(500\ MHz)$ obtained from relaxation dispersion measurements as a function of residue number is shown in Figure 8a for U_{exch} and F_{exch} states (represented as squares and circles, respectively). In this analysis R_{ex} values have been obtained by fitting dispersion profiles to an analytical formula for $R_2^{eff}(\nu_{CP})$ which is exact. For all residues in the F_{exch} state ΔR_{ex} is $\sim$0, indicating that exchange processes other than the slow global folding/unfolding transition are not present. A similar situation is observed for all residues in the U_{exch} state excluding Leu25−Leu28. For these residues ΔR_{ex} deviates significantly from zero, suggesting that intermediate to fast exchange processes contribute to their ^{15}N line widths. Another way to identify intermediate or fast exchange contributions to ^{15}N transverse relaxation is by calculating the static magnetic field strength dependence of the half-step frequency, $\nu_{1/2}$.[21] In the slow exchange limit, $\nu_{1/2}$ scales linearly with $\delta\omega$ and, hence, with B_0, whereas in the fast exchange limit $\nu_{1/2}$ is independent of the chemical shift difference. The ratio of $\nu_{1/2}(800)/\nu_{1/2}(500)$ is plotted as a function of residue number for the F_{exch} and the U_{exch} states in Figure 8b. Residues with additional exchange contributions in the μs−ms regime can be identified by values of $\nu_{1/2}(800)/\nu_{1/2}(500)$ that are smaller than 1.6 and correspond to those amino acids for which nonzero ΔR_{ex} values are observed.

We have used the fact that the N_z experiment senses only the slow folding/unfolding transition, whereas the ^{15}N relaxation dispersion experiment is sensitive to the folding/unfolding transition *and* other intermediate-to-fast exchange events, to separate these processes for residues Leu25−Leu28 in the U_{exch} state of the drkN SH3 domain. Note that the chemical shift differences between residues in the folded and unfolded states, $\delta\omega_{UF}$, are known and that the unfolding and folding rate constants, k_{fu} and k_{uf}, can be obtained from the N_z experiment on a per-residue basis. These values have been used directly in a numerical optimization procedure in which the difference between ex-

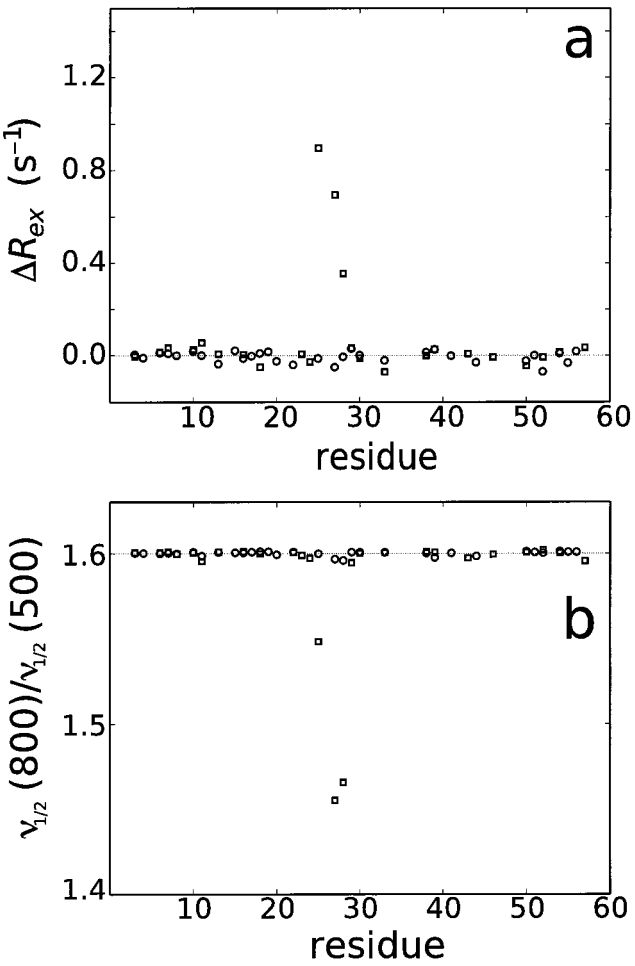

Figure 8. (a) Values of $\Delta R_{ex} = R_{ex}(800\ MHz) - R_{ex}(500\ MHz)$ for residues in the U_{exch} (squares) and F_{exch} states (circles). The straight line drawn at $\Delta R_{ex} = 0.0$ indicates the value of ΔR_{ex} expected if only slow exchange processes contribute to the ^{15}N line width. (b) Values of $\nu_{1/2}(800\ MHz)/\nu_{1/2}(500\ MHz)$ as a function of residue number for residues in the U_{exch} (squares) and F_{exch} (circles) states, respectively. A straight line is drawn at $\nu_{1/2}(800\ MHz)/\nu_{1/2}(500\ MHz) = 1.6$ to indicate the ratio of $\nu_{1/2}(800\ MHz)/\nu_{1/2}(500\ MHz)$ expected for residues exhibiting only slow exchange. Values of R_{ex} and $\nu_{1/2}$ in all cases were determined by fitting dispersion profiles to the exact equation for $R_2^{eff}(\nu_{CP})$ which does not neglect one of the two exponentials describing the evolution of the magnetization (see text).

perimental dispersion profiles (500, 600, and 800 MHz) and calculated profiles describing the three-site exchange process $F \underset{k_{uf}}{\overset{k_{fu}}{\rightleftharpoons}} U \underset{k_{u^*u}}{\overset{k_{uu^*}}{\rightleftharpoons}} U^*$ has been minimized to extract parameters describing the $U \underset{k_{u^*u}}{\overset{k_{uu^*}}{\rightleftharpoons}} U^*$ exchange (see Table 1). The calculated dispersion curves were obtained, in turn, by solving the modified Bloch equations for a three-site exchange system.

Figure 9a shows relaxation dispersion profiles measured at 800 MHz (squares) and 500 MHz (circles) for Thr22 in the U_{exch} state, as a representative example of a residue for which no exchange process other than that associated with global folding/unfolding is observed. In this case the contributions to R_2^{eff} from the $U \underset{k_{u^*u}}{\overset{k_{uu^*}}{\rightleftharpoons}} U^*$ process, illustrated in b (800 MHz) and c (500 MHz) are negligible, and the experimental data is well fit to the exchange model, $F \underset{k_{uf}}{\overset{k_{fu}}{\rightleftharpoons}} U$. This situation is to be contrasted with that observed for Leu25. ^{15}N relaxation dispersion curves for this residue in the U_{exch} state are illustrated in Figure 9d, along with computed R_2^{eff} profiles assuming a simple $F \underset{k_{uf}}{\overset{k_{fu}}{\rightleftharpoons}} U$ exchange process. In this case noticeable residual dispersion is found after subtracting the computed dispersion curves corresponding to the slow folding/unfolding transition (dashed−dot lines) from the experimental relaxation dispersion data. The resulting residual dispersion curves, 800 MHz data (Figure 9e) and 500 MHz data (Figure 9f), reflect conformational exchange processes other than the slow folding/unfolding transition. The residues with statistically significant R_{ex} contributions from intermediate time scale exchange within the U_{exch} state are part of a contiguous segment (Leu25, Ile27, and Leu28). Preliminary studies indicate that the dispersion profile of the subsequent residue, Asn29, also includes contributions from exchange within the unfolded ensemble at temperatures below 20 °C. Unfortunately Lys26 is not amenable to analysis in the U_{exch} state at 20 °C due to spectral overlap. To rule out intermolecular aggregation as the source of the line-broadening observed for residues Leu25−Leu28 in the U_{exch} ensemble a concentration dependence study of peak line width was performed, with the line width found to be independent of protein concentration over the range examined (2−0.5 mM).

A summary of the exchange parameters obtained by simultaneously fitting the relaxation dispersion profiles (upper panels of Figure 9) recorded at ^1H Larmor frequencies of 500, 600, and 800 MHz (for Leu25, Ile27, and Leu28) to a three-site exchange model (see above) is given in Table 1. The static magnetic field dependence of R_{ex} in the free precession limit (cf. $\alpha = d(\ln R_{ex})/d(\ln B_0)$ values[21] in Table 1), indicates that these residues are in intermediate exchange on the NMR chemical shift time scale. For the three residues, Leu25, Ile27, and Leu28, exchange lifetimes vary from 480 ± 80 to 670 ± 130 μs, and the average fractional population of the minor species, p_b, is 0.23 ± 0.02%. The similarity of k_{ex} and p_b values among residues 25−28 in the U_{exch} state suggests that these amino acids are involved in a common exchange process. On the basis of the extracted populations ($K_{eq} = p_b/p_a = 0.0023$) at 20 °C the minor species is 14.8 kJ mol^{-1} (3.5 kcal mol^{-1}) higher in free energy than the unfolded state ensemble at large.

Discussion

^{15}N CPMG-based relaxation dispersion experiments have been employed to study slow dynamic processes in an exchanging F_{exch}/U_{exch} SH3 domain. Excellent agreement between chemical shift differences of resonances in the two states extracted from the ^{15}N relaxation dispersion data, $\delta\omega_{rex}$, and the true chemical shift differences, $\delta\omega_{UF}$, is observed (Figure 6). This result validates the use of the two-state model in fits of the experimental data and indicates the surprising sensitivity of CPMG dispersion profiles to slow exchange processes in cases where the populations of the interconverting species are nearly equal even when exchange contributions, R_{ex}, are small (on average 1.5 s^{-1} for U_{exch} and 0.7 s^{-1} for F_{exch}). Values for the folding and unfolding rate constants, k_{uf} and k_{fu}, can be extracted from the relaxation dispersion data since the exchange contributions to R_2^{eff} (and the oscillations observed in the slow pulsing limit) scale linearly with the rate of interconversion in the slow exchange regime. However, for slowly exchanging systems with small exchange contributions to R_2^{eff}, heteronuclear longitudinal exchange experiments are generally far better suited for obtaining rate constants.

Intermediate Time Scale Dynamics within the U_{exch} Ensemble. In previous studies significant ^{15}N line-broadening has been observed for a contiguous stretch of residues

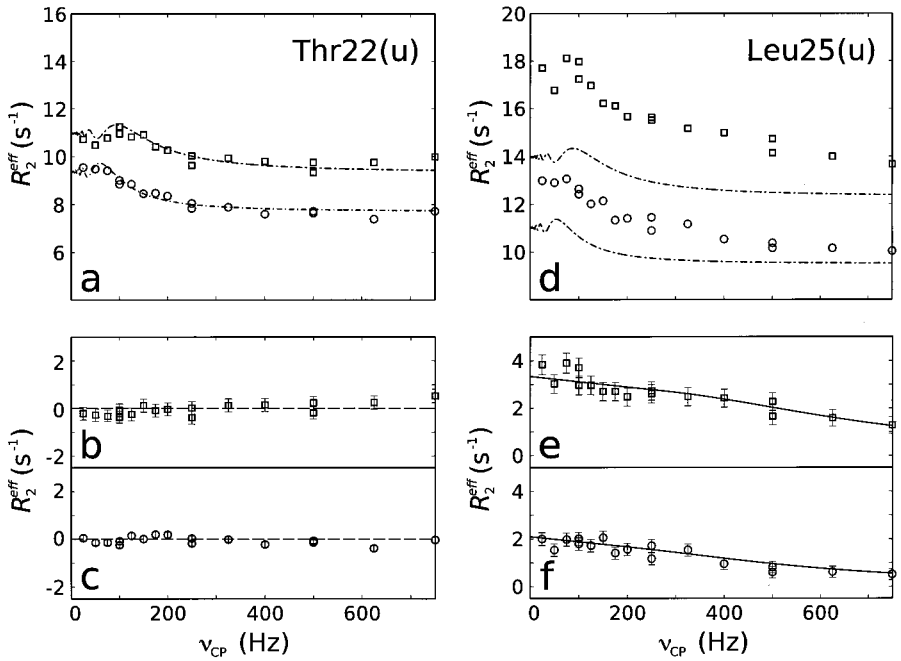

Figure 9. CPMG relaxation dispersion curves for residues Thr22 (a−c) and Leu25 (d−f) in the drkN SH3 domain U_{exch} state. Panels a and d show experimental values of R_2^{eff} as a function of the CPMG field strength with data recorded at 800 (500) MHz ^{1}H Larmor frequency indicated with squares (circles); data recorded at 600 MHz are not shown but used for the analysis. A three-site exchange model corresponding to the process $F \underset{k_{uf}}{\overset{k_{fu}}{\rightleftharpoons}} U \underset{k_{u^*u}}{\overset{k_{uu^*}}{\rightleftharpoons}} U^*$ is used to fit the experimental $R_2^{eff}(\nu_{CP})$ profiles. Values for k_{UU^*}, k_{U^*U}, $\delta\omega_{UU^*}$, and $R_2(\infty)$ are obtained from the fits using $\delta\omega_{UF}$, k_{uf}, and k_{fu} set to values determined for each residue individually from the N_z experiment. The best-fit values (Table 1) are subsequently used to calculate dispersion profiles corresponding to the slow folding−unfolding transition only. To calculate these curves, Bloch equations for three-site chemical exchange are solved with $\delta\omega_{UU^*}$ set to zero. The resulting profiles are illustrated with dashed−dot lines in panels a and d with the upper line corresponding to $R_{2,slow}^{eff}(\nu_{CP})$ at 800 MHz and the lower line to $R_{2,slow}^{eff}(\nu_{CP})$ at 500 MHz. Panels b, c (Thr22) and e, f (Leu25) show the difference between experimental dispersion data and computed dispersion contributions due to the slow folding−unfolding transition (dashed−dot lines in panels a and d) at 800 MHz (squares) and 500 MHz (circles), reflecting μs−ms time scale events only. For Thr22 (no local exchange on an intermediate time scale), a dashed straight line is drawn to guide the eye. For Leu25, contributions from the $U \underset{k_{u^*u}}{\overset{k_{uu^*}}{\rightleftharpoons}} U^*$ equilibrium are modeled by solving Bloch equations for three-site exchange with $\delta\omega_{UF}$ set to zero (solid lines; e, 800 MHz data and f, 500 MHz data). Only residues 25−28 in the U_{exch} state were found to show statistically significant contributions to the ^{15}N line width from the intermediate time scale exchange process.

Table 1. ^{15}N Relaxation Dispersion Parameters for the Intermediate Time Scale Exchange Process in the U_{exch} State of the drkN SH3 Domain at 20 °C[a]

	p_b (%)[b]	τ_{ex} (ms)	$\delta\omega_{UU^*}$ (ppm)	α-value[c]
Leu25	0.25 ± 0.01	0.47 ± 0.08	6.6 ± 1.9	0.93 ± 0.09
Ile27	0.21 ± 0.03	0.67 ± 0.13	5.9 ± 2.0	0.68 ± 0.19
Leu28	0.22 ± 0.02	0.60 ± 0.08	7.2 ± 2.3	0.54 ± 0.12

[a] Parameters were extracted by fitting the relaxation dispersion data at 500, 600, and 800 MHz ^{1}H Larmor frequencies simultaneously to a model of the 3-site chemical exchange process using the known values of $\delta\omega_{UF}$, k_{uf}, and k_{fu} for the slow folding/unfolding transition. A Monte Carlo approach was used to obtain the errors in the parameters extracted from the fit, estimating experimental uncertainties in R_2^{eff} from the three duplicate measurements. [b] Population of the minor conformer.[c] $\alpha = d(\ln R_{ex})/d(\ln B_0)$ where $R_{ex} = [R_2^{eff}(1/\tau_{CP} \rightarrow 0) - R_2^{eff}(1/\tau_{CP} \rightarrow \infty)]$[21] (see Figure 9, e and f).

(23−28) in the U_{exch} ensemble of the drkN SH3 domain under nondenaturing conditions, which is increased by reducing the temperature.[32] The presence of μs−ms time scale dynamics for this segment of the protein is supported by ^{15}N relaxation studies on a guanidinium chloride destabilized state of the molecule (U_{Gdn}), in which spectral density mapping analysis established that spectral density values evaluated at zero frequency for Leu25 and Leu28 are noticeably larger than those of neighboring residues, consistent with a contribution to the ^{15}N transverse relaxation rate from conformational exchange.[38]

The similarity of the exchange parameters obtained for residues in the contiguous region between Leu25−Leu28 in the U_{exch} state indicates that these residues are involved in a common exchange process and that the relevant motions are locally collective. We have noted previously that residues between 24 and 28 correspond to a local minimum in a hydrophilicity plot.[38] Hydrophobic residues are more likely to be restricted in their motion in aqueous solution than hydrophilic residues, with a tendency for local hydrophobic collapse. In the folded state residues 25−28 form a β-strand that makes interstrand hydrogen bonds with two neighboring strands. Together these three strands comprise a regular three-stranded antiparallel β-sheet, with the side chains of residues 25−28 oriented toward opposite faces of the β-sheet. Hence, a local hydrophobic collapse involving these residues in the U_{exch} state would be non-native. Such non-native interactions could slow the exchange of these conformational states with the rest of the unfolded ensemble, which likely consists of more nativelike conformations rapidly interconverting. The low population of the minor substate (0.23 ± 0.02%) indicates that its free energy is ∼3.5 kcal mol^{-1} higher than for the major component of the U_{exch} state with the probable gain in stabilization due to enthalpic interactions in this substate presumably overcome by lowering of entropy.

The low population of the minor substate makes it difficult to study by conventional NMR methods; indeed, relaxation dispersion spectroscopy is one of the few methods that is sensitive to the presence of such low-populated states. Other NMR data on the drkN SH3 domain and computational

(38) Farrow, N. A.; Zhang, O.; Forman-Kay, J. D.; Kay, L. E. *Biochemistry* **1997**, *36*, 2390−2402.

predictions using the program AGADIR1s[39] indicate a pronounced α-helical propensity (>10%) for residues 15−28.[40] This is consistent with H^{α} and C^{α} secondary chemical shifts, $^3J_{HNH_\alpha}$ coupling constants, and NOE data which provide evidence that residues in this region of the protein indeed sample the α-region of ϕ,ψ-space.[32] However, the intermediate time scale exchange process in the region encompassing residues Leu25−Leu28, which is sensed by the ^{15}N CPMG relaxation dispersion experiment, almost certainly does not correspond to the interconversion between random-coil structures and α-helical-like conformation. This is because (i) the populations obtained from fitting the experimental data are too small to explain the chemical shift, *J*-coupling, or NOE data and (ii) ^{15}N line-broadening is not observed for residues 15−22. The extremely low value of the $^3J_{HNH_\alpha}$ coupling constant found for Leu28 in the U_{exch} state (at 30 °C), for instance, cannot be explained by the presence of a minor species with a population <0.3%.[28] In addition, helix−coil transitions most likely occur on a time scale too fast (<1 μs) to be amenable to investigation by ^{15}N CPMG relaxation dispersion experiments.[41] It is interesting to note, however, that several clusters of hydrophobic residues were found in a structure calculated for the U_{exch} state, from long-range NOE data, with one of these hydrophobic clusters comprising the side chains of residues Ile24−Leu28.[30]

It should be mentioned that ^{15}N relaxation dispersion experiments which make use of the CPMG approach are most sensitive to exchange processes with time constants on the order of ms, with appreciable populations of the minor state(s) and with reasonably large chemical shift differences between the corresponding states. It is likely that other transient interactions are present in the U_{exch} state of the drkN SH3 domain but that the corresponding exchange processes cannot be sensed by the ^{15}N relaxation dispersion experiments performed in this study. Nevertheless, the technique remains an extremely useful tool for characterizing conformational ensembles with a remarkable sensitivity to very small populations of substates.

Conclusions

We have utilized the CPMG relaxation dispersion technique to study conformational exchange processes in the F_{exch}/U_{exch} system of the drkN SH3 domain. Results demonstrate the applicability of this approach for the investigation of exchange processes on a time scale of ∼500 ms involving sites with similar equilibrium populations. Typically these events are studied by monitoring the exchange of longitudinal magnetization. An analytical expression for the dependence of the effective transverse relaxation rate on the CPMG field strength for a two-site exchanging system in the limit of slow exchange has been derived and used to analyze the global folding/unfolding transition between the F_{exch} and U_{exch} states.

In addition, the relaxation dispersion experiments indicate the presence of intermediate time scale exchange involving a very sparsely populated substate within the U_{exch} ensemble composed of several contiguous hydrophobic residues which is likely formed due to local hydrophobic collapse. The rate of exchange and the fractional population have been determined for this substate. The high sensitivity of the CPMG dispersion measurements to small populations (<0.3%) underscores the utility of the approach for quantitative characterization of dynamic ensembles.

Materials and Methods

Sample Conditions and NMR Measurements. Samples of ^{15}N-labeled drkN SH3 domain were prepared as described previously.[28] Sample conditions were: 1.9 mM protein (^{15}N CT-CPMG relaxation dispersion experiments) or 1.1 mM protein (N_z exchange experiments), 0.05 M sodium phosphate, 90% H_2O/10% D_2O, pH 6. All NMR spectra were recorded at 20 °C on Varian Inova spectrometers. Relaxation dispersion data were obtained at three static magnetic fields, corresponding to proton Larmor frequencies of 500, 600, and 800 MHz using a relaxation-compensated CPMG dispersion experiment[22] performed in a constant time manner (Figure 1). Spectra were collected as a series of 14 2D data sets with CPMG field strengths, ν_{CP}, of 25, 50, 75, 100, 125, 150, 175, 200, 250, 325, 400, 500, 625, and 750 Hz, with repeat experiments performed at CPMG field strengths of 100, 250, and 500 Hz and reference spectra obtained by omitting the CPMG period in the pulse sequence, as described by Mulder et al.[23] Each 2D spectrum was recorded as a complex data matrix comprised of 96 × 768 points, 108 × 768 points, or 116 × 768 points at 500, 600, and 800 MHz ^1H Larmor frequencies, respectively. 24 scans per FID were recorded, with a recycle delay of 2.2 s, giving rise to a net acquisition time of approximately 3 h/data set. The CT delay was set to $T_{CP} = 80$ ms to allow for sufficient sampling of the relaxation dispersion curves at low CPMG field strengths. Data were processed and analyzed using NMRPipe software.[42] Peak intensities were measured as the sum of the intensities in a 3 × 3 grid centered on the peak maximum. The intensities of cross-peaks were then converted into decay rates, R_2^{eff}, for a given CPMG field strength, ν_{CP}, as described previously.[23] *F*-test criteria[43] were used to assess the statistical significance of including an R_{ex} term in the fit as opposed to flat-line fits, using 99.9% confidence limits.

The N_z experiment used for simultaneous measurement of chemical exchange and longitudinal ^{15}N decay rates[29] was performed at 800 MHz. A series of 13 2D spectra was collected with mixing times ranging from 11 to 691 ms, with four repeat experiments. Each 2D spectrum was recorded as a complex data matrix composed of 128 × 768 points. Forty-eight scans per FID were obtained, with a recycle delay of 1.2 s (3−4.5 h/data set). To analyze the data properly the different relaxation properties of magnetization associated with the unfolded and folded states must be taken into account. With reference to the pulse sequence shown in Figure 1 of Farrow et al.,[29] we can write the dependence of auto (*ff*,*uu*)- and cross (*fu*,*uf*)-peak volumes on the variable mixing period, *T*, as:

$$I_{ff}(T)/I_{ff}(0) = A_f(-(\lambda_2 - a_{11})\,e^{-\lambda_1 T} + (\lambda_1 - a_{11})\,e^{-\lambda_2 T})/(\lambda_1 - \lambda_2)$$
$$I_{uu}(T)/I_{uu}(0) = A_u(-(\lambda_2 - a_{22})\,e^{-\lambda_1 T} + (\lambda_1 - a_{22})\,e^{-\lambda_2 T})/(\lambda_1 - \lambda_2) \quad (3)$$
$$I_{fu}(T)/I_{ff}(0) = A_u(a_{21}\,e^{-\lambda_1 T} - a_{21}\,e^{-\lambda_2 T})/(\lambda_1 - \lambda_2)$$
$$I_{uf}(T)/I_{uu}(0) = A_f(a_{12}\,e^{-\lambda_1 T} - a_{12}\,e^{-\lambda_2 T})/(\lambda_1 - \lambda_2)$$

where $\lambda_{1,2} = {}^1/_2\{(a_{11} + a_{22}) \pm [(a_{11} - a_{22})^2 + 4\,k_{fu}k_{uf}]^{1/2}\}$, $a_{11} = R_{1f} + k_{fu}$, $a_{12} = -k_{uf}$, $a_{22} = R_{1u} + k_{uf}$, $a_{21} = -k_{fu}$. R_{1u} and R_{1f} are the longitudinal relaxation rate constants of magnetization in sites *u* and *f*,

(39) Munoz, V.; Serrano, L. *J. Mol. Biol.* **1995**, *245*, 275−296.
(40) Blanco, F. J.; Serrano, L.; Forman-Kay, J. D. *J. Mol. Biol.* **1998**, *284*, 1153−1164.
(41) Eaton, W. A.; Munoz, V.; Hagen, S. J.; Jas, G. S.; Lapidus, L. J.; Henry, E. R.; Hofrichter, J. *Annu. Rev. Biophys. Biomol. Struct.* **2000**, *29*, 327−359.
(42) Delaglio, F.; Torchia, D. A.; Bax, A. *J. Biomol. NMR* **1991**, *1*, 439−476.
(43) Bevington, P. R.; Robinson, D. K. *Data Reduction and Error Analysis for the Physical Sciences*; WCB/McGraw-Hill: New York, 1992.
(44) Geen, H.; Freeman, R. *J. Magn. Reson.* **1991**, *93*, 93−141.
(45) Piotto, M.; Saudek, V.; Sklenar, V. *J. Biomol. NMR* **1992**, *2*, 661−665.
(46) Shaka, A. J.; Keeler, J.; Frenkiel, T.; Freeman, R. *J. Magn. Reson.* **1983**, *124*, 355−365.
(47) Marion, D.; Ikura, M.; Tschudin, R.; Bax, A. *J. Magn. Reson*. **1989**, *85*, 393−399.
(48) Kay, L. E.; Keifer, P.; Saarinen, T. *J. Am. Chem. Soc.* **1992**, *114*, 10663−10665.
(49) Schleucher, J.; Sattler, M.; Griesinger, C. *Angew. Chem., Int. Ed. Engl.* **1993**, *32*, 1489−1491.

respectively, and $I_{uu}(0)$ and $I_{ff}(0)$ denote the longitudinal nitrogen magnetization associated with the unfolded and folded states at the start of the mixing time. Factors A_u and A_f represent the efficiency of coherence transfer, $^{15}N \rightarrow {}^{1}H$, during the reverse INEPT steps (the final two periods of the sequence of Figure 1 in Farrow et al.[29] with delays $2\tau_c$ and $2\tau_a$) for magnetization associated with the unfolded and folded state, respectively. As long as the delays $2\tau_c$ and $2\tau_a$ are multiples of $1/(2J_{NH})$, A_u and A_f are given by $A_f = \exp[-(R^{avg}_{2N,f}2\tau_c + R^{avg}_{2H,f}2\tau_a)]$ and $A_u = \exp[-(R^{avg}_{2N,u}2\tau_c + R^{avg}_{2H,u}2\tau_a)]$, where $R^{avg}_{2N,f}$ ($R^{avg}_{2N,u}$) and $R^{avg}_{2H,f}$ ($R^{avg}_{2H,u}$) are averages of the transverse relaxation rates for in-phase and anti-phase ^{15}N and ^{1}HN magnetization associated with the folded (unfolded) state. $R^{avg}_{2N,f}$, $R^{avg}_{2N,u}$ can be obtained on a per-residue basis by recording a pair of spectra with $2\tau_c = 2\tau_a = 1/(2J_{NH})$ and $2\tau_c = 3/(2J_{NH})$, $2\tau_a = 1/(2J_{NH})$ and comparing peak intensities. In a similar way, $R^{avg}_{2H,f}$, $R^{avg}_{2H,u}$ can be measured by recording a set of spectra where the last $2\tau_a$ delay in Figure 1 of Farrow et al.[29] is set to $\{1/(2J_{NH}), 3/(2J_{NH})\}$, with $2\tau_c = 1/(2J_{NH})$ in both cases. Note that the delays $2\tau_c$ and $2\tau_a$ must be set to exactly $1/(2J_{NH})$ or $3/(2J_{NH})$ to ensure complete averaging of in-phase and anti-phase relaxation during each of the $2\tau_c$ and $2\tau_a$ periods; these values were also employed in the N_z experiment. Differential relaxation losses prior to the mixing period do not need to be accounted for in the same way since they are subsumed in the constants $I_{uu}(0)$ and $I_{ff}(0)$.

To extract values for k_{uf}, k_{fu}, R_{1u} and R_{1f} we have fitted the experimental curves for $I_{ff}(T)$, $I_{uu}(T)$, $I_{fu}(T)$ and $I_{uf}(T)$ simultaneously using a least-squares fitting procedure, with errors estimated by a Monte Carlo analysis based on the four repeat experiments. In principle, peak volumes, not heights, must be used for $I(T)$ values, since differences in line widths between peaks originating from magnetization associated with the folded and unfolded states do arise. We have found that it is difficult to extract accurate peak volumes for short values of T and have therefore used the product of measured peak heights with residue specific ^{1}HN line widths obtained by fitting a Lorentzian function to the auto peaks to approximate the volumes. Note that differences in ^{15}N line widths are taken into account automatically by including the residue-specific fitting parameters, $I_{uu}(0)$ and $I_{ff}(0)$. Because exchange cross-peaks were not observed in experiments with zero mixing time, magnetization transfer between the folded and unfolded states due to exchange during the reverse INEPT elements after the mixing period was not taken into account in our analysis.

Appendix: Derivation of Equation 2

Consider a spin I exchanging between two sites, A and B, with magnetization modes M_a and M_b corresponding to the single-quantum coherences $I_+(a)$ and $I_+(b)$, respectively. The evolution of M_a and M_b is given by the solution to

$$\frac{d}{dt}\begin{bmatrix}M_a(t)\\M_b(t)\end{bmatrix} = \begin{bmatrix}-(R_{2a}+k_a) & k_b\\ k_a & -(R_{2b}+k_b+i\delta\omega)\end{bmatrix}\begin{bmatrix}M_a(t)\\M_b(t)\end{bmatrix} \quad \text{(A1)}$$

where $\delta\omega$ is the offset between the two resonance frequencies and R_{2a}, R_{2b} are the respective relaxation rates of modes M_a and M_b. We shall now seek the approximate solution of eq A1 in the following form

$$\begin{bmatrix}M_a(2n\tau_{CP})\\M_b(2n\tau_{CP})\end{bmatrix} = \{\Lambda(4\tau_{CP})\}^{n/2}\begin{bmatrix}M_a(0)\\M_b(0)\end{bmatrix} \quad \text{(A2)}$$

where the matrix $\Lambda(4\tau_{CP})$ describes the evolution of the system during the $(\tau_{CP}-180°-2\tau_{CP}-180°-\tau_{CP})$ element of the CPMG sequence. In the derivation it is assumed that the slow exchange condition is fulfilled

$$k_a, k_b \ll \delta\omega \quad \text{(A3.1)}$$

and that the τ_{CP} interval is short enough to justify the use of the following approximations,

$$R_{2a}, R_{2b}, k_a, k_b \ll 1/\tau_{CP} \quad \text{(A3.2)}$$

Integrating the first line from the system of equations, eq A1, over the first τ_{CP} interval we obtain

$$M_a(\tau_{CP}) = M_a(0) - (R_{2a}+k_a)\int_0^{\tau_{CP}} M_a(0)dt + k_b\int_0^{\tau_{CP}} M_b(0)\, e^{-i\delta\omega t}dt \quad \text{(A4.1)}$$

to linear approximation. In eq A4.1 it has been assumed that to the zeroth order the evolution of $M_b(t)$ is given by $M_b(t) = M_b(0)\exp(-i\delta\omega t)$. The 180° pulse has the effect of converting $I_+(a)$, $I_+(b)$ into $I_-(a)$, $I_-(b)$ with concomitant reversal of the chemical shift evolution. Hence, extending the integration to the second τ_{CP} interval yields

$$M_a(2\tau_{CP}) = M_a(0) - (R_{2a}+k_a)\int_0^{2\tau_{CP}} M_a(0)dt + k_b\left(\int_0^{\tau_{CP}} M_b(0)\, e^{-i\delta\omega t}dt + \int_0^{\tau_{CP}} M_b(0)\, e^{-i\delta\omega(\tau_{CP}-t)}dt\right) \quad \text{(A4.2)}$$

After the integration is performed in the same manner over the third and fourth τ_{CP} intervals, the matrix $\Lambda(4\tau_{CP})$, eq A2, can be expressed as

$$\Lambda(4\tau_{CP}) \cong \begin{bmatrix}1-4(R_{2a}+k_a)\tau_{CP} & 4(k_b/\delta\omega)\sin(\delta\omega\tau_{CP})\\ 4(k_a/\delta\omega)\sin(\delta\omega\tau_{CP}) & 1-4(R_{2b}+k_b)\tau_{CP}\end{bmatrix} \quad \text{(A5)}$$

Raising this matrix to the power $n/2$, eq A2, we retain only the terms linear with respect to the parameters R_{2a}, R_{2b}, k_a, k_b, (see eq A3) arriving at,

$$\begin{bmatrix}M_a(2n\tau_{CP})\\M_b(2n\tau_{CP})\end{bmatrix} \cong \begin{bmatrix}1-2n(R_{2a}+k_a)\tau_{CP} & 2n(k_b/\delta\omega)\sin(\delta\omega\tau_{CP})\\ 2n(k_a/\delta\omega)\sin(\delta\omega\tau_{CP}) & 1-2n(R_{2b}+k_b)\tau_{CP}\end{bmatrix}\begin{bmatrix}M_a(0)\\M_b(0)\end{bmatrix} \quad \text{(A6)}$$

Finally, utilizing the chemical balance condition, $k_aM_a(0) = k_bM_b(0)$ and recalling that $1-\lambda t \approx \exp(-\lambda t)$, we obtain from the first line of eq A6 the expression for the effective relaxation rate constant which describes the attenuation of magnetization during the variable-spacing constant-time CPMG period,

$$R^{eff}_{2a} = R_{2a} + k_a - k_a\frac{\sin(\delta\omega\tau_{CP})}{\delta\omega\tau_{CP}} \quad \text{(A7)}$$

The conditions of validity for the above equations are given in eq A3. It is worth noting that in the limit that $\nu_{CP} \rightarrow \infty$ (spin-locking condition), eq A7 predicts that $R^{eff}_{2a} = R_{2a}$. In fact, this case can be treated separately by assuming that the chemical shift difference is quenched by a strong spin-locking field. Such a treatment predicts a correction to R^{eff}_{2a} in this limit that is dependent on R_{2b}. From this consideration it follows that eq A7 holds for large ν_{CP} values only for the case that $|R_{2a} - R_{2b}| \ll k_a, k_b$.

Equation A7 has been verified using the exact analytical solution of eq A2 generated with the help of the symbolic computation program Maple (Waterloo Maple Inc.). This solution was obtained using the analytical expressions for the eigenvalues and eigenvectors of the matrix in eq A1. The evolution matrix $\Lambda(4\tau_{CP})$ calculated in this manner was subsequently transformed into diagonal form and raised to the power $n/2$. The resulting analytical formula for R^{eff}_2 was stored as

FORTRAN or Matlab (MathWorks Inc.) code and used in fitting the dispersion data.

Acknowledgment. We thank Dr. O. Millet (University of Toronto) for many helpful discussions, Dr. Ranjith Muhandiram (University of Toronto) for help in setting up the experiments, and Dr. Karin Kloiber (University of Innsbruck) for assistance with simulations. We acknowledge Dr. H.-S. Chan for useful discussions. The research was supported by grants from the Medical Research Council of Canada (J.D.F.-K. and L.E.K.) and the Natural Sciences and Engineering Research Council of Canada (L.E.K.). M.T. and F.A.A.M are the recipients of an E. Schrodinger Fellowship (J-1933-GEN) of the Austrian Science Fund and a postdoctoral stipend from the European Molecular Biology Organization, respectively. N.R.S. acknowledges a Centennial Fellowship from the Medical Research Council of Canada. L.E.K. is a foreign investigator of the Howard Hughes Medical Research Institute. Support from AstraZeneca is gratefully acknowledged. The exact analytical solution of eq A2 (see Appendix) is available from the authors upon request.

Supporting Information Available: Table of $\delta\omega_{rex}$ obtained from fits of relaxation dispersion profiles recorded at 500, 600, and 800 MHz and Table of k_{uf}, k_{fu} obtained from the N_z exchange experiment (PDF). This material is available free of charge via the Internet at http://pubs.acs.org.

JA011300Z